LBL-36995
UC-1600

A New Method for Predicting the Solar Heat Gain of Complex Fenestration Systems

J.H. Klems, J.L. Warner, and G.O. Kelley

March 1995

Prepared for the U.S. Department of Energy under Contract Number DE-AC03-76SF00098

DISCLAIMER

Available to DOE and DOE Contractors
from the Office of Scientific and Technical Information
P.O. Box 62, Oak Ridge, TN 37831
Prices available from (615) 576-8401

Available to the public from the
National Technical Information Service
U.S. Department of Commerce
5285 Port Royal Road, Springfield, VA 22161

Lawrence Berkeley National Laboratory
is an equal opportunity employer.

LBL-36995
TA-335

ASHRAE Solar Heat Gain Project 548 - RP. Final Report

A New Method for Predicting the Solar Heat Gain of Complex Fenestration Systems

J. H. Klems, J.L. Warner, and G.O. Kelley

Building Technologies Program
Energy and Environment Division
Lawrence Berkeley Laboratory
University of California
Berkeley, California 94720

March 1995

This research was jointly supported by ASHRAE, as Research Project 548-RP under Agreement No. BG 87-127 with the U.S. Department of Energy, and by the Assistant Secretary for Energy Efficiency and Renewable Energy, Office of Building Technologies, Building Systems and Materials Division of the U.S. Department of Energy under Contract No. DE-AC03-76SF00098.

ASHRAE Solar Heat Gain Project 548-RP

Final Report

A New Method for Predicting the Solar Heat Gain of Complex Fenestration Systems

J. H. Klems, J. L. Warner and G. O. Kelley

Building Technologies Program

Lawrence Berkeley Laboratory

Berkeley, CA 94720

Abstract

A new method of predicting the solar heat gain through complex fenestration systems involving nonspecular layers such as shades or blinds has been examined in a project jointly sponsored by ASHRAE and DOE. In this method, a scanning radiometer is used to measure the bi-directional radiative transmittance and reflectance of each layer of a fenestration system. The properties of systems containing these layers are then built up computationally from the measured layer properties using a transmission/multiple-reflection calculation. The calculation produces the total directional-hemispherical transmittance of the fenestration system and the layer-by-layer absorptances. These properties are in turn combined with layer-specific measurements of the inward-flowing fractions of absorbed solar energy to produce the overall solar heat gain coefficient.

The method has been applied to one of the most optically complex systems in common use, a venetian blind in combination with multiple glazings. A comparison between the scanner-based calculation method and direct system calorimetric measurements made on the LBL MoWiTT facility showed good agreement, and is a significant validation of the method accuracy and feasibility.

Introduction

This report summarizes the work on ASHRAE Research Project 548-RP. The detailed results of the project are described in four technical publications(Klems and Warner 1992; Klems 1994A; Klems 1994B; Klems and Warner 1995) and two draft publications(Klems and Kelley 1995; Klems, Warner et al. 1995). Additional output is contained in a publicly available data base of measurements maintained at Lawrence Berkeley Laboratory (LBL).

The goal of this research project was to develop a method for characterizing the performance of glazing systems containing optically complex elements, such as venetian blinds, shades, or other nonspecular shading devices, and to demonstrate the feasibility of this method by accumulating the data necessary to apply the method and comparing the resulting prediction of solar heat gain coefficient (SHGC) with measurements made under realistic conditions.

Strategy and Scope of the Project

Beginning with the standard definition of the SHGC, F, extension to a multilayer complex glazing system requires an F that may depend (in the most complex case) on two angles (θ,ϕ) specifying the input direction. The incident angle, q, is the angle between the incident rays and the normal to the plane of the glazings. When one of the fenestration elements has a characteristic direction in the glazing plane (e.g., the direction of venetian blind slats), then F may also depend on the azimuthal angle, f, of the plane of incidence (the plane containing both the incident direction and the normal to the glazing plane) relative to that characteristic direction. In the general case, then, the SHGC is given by

$$F(\theta,\phi) = T_{fH}(\theta,\phi) + \sum_{i=1}^{M} N_i A_{fi}(\theta,\phi), \qquad (1)$$

where T_{fH} is the directional-hemispherical solar-optical transmittance of the system, it is assumed that there are M layers, A_{fi} is the front absorption and N_i the inward-flowing fraction (IFF) of the *i* th layer. For determining F the project methodology utilizes two strategies, which we term *thermal-solar separation* and *the layer method:* (1) *Thermal-solar separation:* N_i must be determined calorimetrically for a given system geometry and set of emittances, but will be the same for all such systems regardless of the solar-optical properties of the layers. It therefore need only be determined once for a "thermally prototype" system and can be combined with quantities T_{fH} and A_{fi} determined by non-calorimetric optical techniques to produce values of F for a variety of similar systems. (2) *The layer method:* T_{fH} and A_{fi}, which are system solar-optical properties (A_{fi} being the layer absorptance in a given system), are calculated from the bi-directional transmittance and reflectance distribution functions of individual layers.

In addition the project characterizes complex layer bi-directional properties by a measurement of their spatially-averaged characteristics over a suitably chosen grid of discrete directions.

This strategy represents an extreme position on what is really a continuum of possible characterization strategies, all of which share the necessary condition of solar-thermal separation. Since, in principle, measurement of spatially averaged properties can be applied to any shading or sun-control device of reasonably modular construction (overhangs and awnings, which do not fall in this class, may be adequately treated with already-existing calculation methods), a successful proof-of concept of this method will also, by demonstrating the viability of solar-optical separation, support the validity of

intermediate methods. As will be seen, nearly any subsystem may be designated as a layer and assigned layer bi-directional properties that may be determined in a variety of ways.

The value of thermal-solar separation is that it limits calorimetry, which is a laborious and time-consuming measurement, to the minimal generic characterization of systems, allowing solar-optical differences (such as color or design, which may have architectural importance) to be characterized by simpler and faster optical measurement and/or calculational techniques. The layer method, in turn, allows the concentration of measurement or calculational effort on the part of a system that has truly complicated solar-optical properties without having to treat it in multiple combinations with simpler optical elements. For example, a venetian blind, which is optically complex, may be combined in various ways with multiple panes of glass of varying tints and coatings, (assumed here not to differ in emissivity) all of which are optically simple, *i.e.*, specular. The layer method allows one to characterize the blind separately, to calculate the glazing layer properties from normally available spectrophotometric data, and to form the combinations with the glazings by calculations. Intermediate methods (*e.g.*, measurement in an integrating sphere) might require the separate determination of properties (*e.g.*, direct measurement of T_{fH} and A_{fi} in equation 1) for each combination of blind and distinct glazings.

In practice, experience alone will determine which methods are most effective and economical for characterizing specific systems. Calculations of overall SHGC could show that some systems might be characterized to sufficient accuracy by a very simple model with a few characteristics to be determined by measurement. For example, it might prove adequate to characterize a shade as a perfectly diffuse reflector and transmitter (or perhaps having some other, theoretical, distribution). In that case an integrating sphere measurement to determine overall reflectance and transmittance of the shade would be sufficient. A fixed louver system might be characterizable as a combination of (incident-direction-dependent) specular transmitter and diffuse reflector/transmitter; or, alternatively, it might be possible to compute its complete bi-directional layer properties from its geometric shape and measurements of the bi-directional relectance distribution function (BRDF) of its surfaces. Again, a device that either could not be disassembled or had poorly controlled variable aspects to its construction (variations in venetian blind slat positioning and shapes come to mind) might require spatially-averaged layer bi-directional measurements either on a single sample or a representative set of samples (to determine mean properties and variability).

The point is that, once the validity of thermal-solar separation is established and the layer method is taken as an overall starting point, all of these various solar-optical characterization strategies may be accommodated within the overall calculational framework, since a "layer" is effectively any subsystem that is conveniently treated as a unit with planar surfaces. In addition, the same thermal prototype systems that must have N_j values determined by heat transfer methods (calorimetry, or possibly hotbox, measurements or detailed thermal models) also have a thermal transmittance (U-factor) that similarly obeys thermal-solar separation and may be determined by the same method. The U-factor appears to be more sensitive to the thermal properties than N_j (the layer IFF).

The Layer Method

In the layer method, the fenestration system is broken up into a series of plane-parallel layers. The outgoing radiance from a layer is characterized by its distribution over a finite grid of directions, specified by angular coordinates $\left(\theta_0^{(l)}, \phi_0^{(l)}\right)$, where the superscript l runs over all of the grid elements. This information is arranged into a column vector of outgoing radiance:

$$\mathbf{I} = \begin{pmatrix} I(\theta_0^{(1)}, \phi_0^{(1)}) \\ I(\theta_0^{(2)}, \phi_0^{(2)}) \\ \cdots \\ I(\theta_0^{(N)}, \phi_0^{(N)}) \end{pmatrix}. \tag{2}$$

The number of elements in (*i.e.*, the dimension of) the column vector depends on the number of directions necessary to specify the output radiance sufficiently. For example, for a highly diffusing layer for which the outgoing radiance does not depend greatly on the incident direction, our scheme would use seven elements; for the most complex layer it uses 145. More or fewer elements could be used as experience dictates.

Each direction in the grid characterizes an element of solid angle, $\Delta\Omega^{(l)}$, and these are arranged in a diagonal matrix, called a propagation matrix,

$$\mathbf{\Lambda} = \begin{pmatrix} \Delta\Omega^{(1)} \cos(\theta^{(1)}) & 0 & \cdots & 0 \\ 0 & \Delta\Omega^{(2)} \cos(\theta^{(2)}) & 0 & \cdots \\ \cdots & 0 & \cdots & 0 \\ 0 & \cdots & 0 & \Delta\Omega^{(N)} \cos(\theta^{(N)}) \end{pmatrix}, \tag{3}$$

so that the incoming irradiance, E, at the next layer (a column vector) can be calculated by matrix multiplication,

$$\mathbf{E} = \begin{pmatrix} E(\theta^{(1)}, \phi^{(1)}) \\ E(\theta^{(2)}, \phi^{(2)}) \\ \cdots \\ E(\theta^{(N)}, \phi^{(N)}) \end{pmatrix} = \mathbf{\Lambda} \cdot \mathbf{I} = \begin{pmatrix} \Delta\Omega^{(1)} \cos(\theta^{(1)}) \cdot I(\theta^{(1)}, \phi^{(1)}) \\ \Delta\Omega^{(2)} \cos(\theta^{(2)}) \cdot I(\theta^{(2)}, \phi^{(2)}) \\ \cdots \\ \Delta\Omega^{(N)} \cos(\theta^{(N)}) \cdot I(\theta^{(N)}, \phi^{(N)}) \end{pmatrix}. \tag{4}$$

The bi-directional transmittance distribution function (BTDF) of a layer, $\tau(\theta_0^{(l)}, \phi_0^{(l)}; \theta_1^{(m)}, \phi_1^{(m)})$, where τ denotes transmittance from an incoming grid direction $(\theta_1^{(m)}, \phi_1^{(m)})$ to an outgoing grid direction $(\theta_0^{(l)}, \phi_0^{(l)})$, is arranged into a transmittance matrix,

$$\boldsymbol{\tau} = \begin{pmatrix} \tau(\theta_0^{(1)}, \phi_0^{(1)}; \theta_1^{(1)}, \phi_1^{(1)}) & \tau(\theta_0^{(1)}, \phi_0^{(1)}; \theta_1^{(2)}, \phi_1^{(2)}) & \dots & \tau(\theta_0^{(1)}, \phi_0^{(1)}; \theta_1^{(N)}, \phi_1^{(N)}) \\ \tau(\theta_0^{(2)}, \phi_0^{(2)}; \theta_1^{(1)}, \phi_1^{(1)}) & \tau(\theta_0^{(2)}, \phi_0^{(2)}; \theta_1^{(2)}, \phi_1^{(2)}) & \dots & \tau(\theta_0^{(2)}, \phi_0^{(2)}; \theta_1^{(N)}, \phi_1^{(N)}) \\ \dots & \dots & \dots & \dots \\ \tau(\theta_0^{(N)}, \phi_0^{(N)}; \theta_1^{(1)}, \phi_1^{(1)}) & \tau(\theta_0^{(N)}, \phi_0^{(N)}; \theta_1^{(2)}, \phi_1^{(2)}) & \dots & \tau(\theta_0^{(N)}, \phi_0^{(N)}; \theta_1^{(N)}, \phi_1^{(N)}) \end{pmatrix}, \quad (5)$$

so that the outgoing radiance distribution, I, from a layer with an incident irradiance E is calculated by simple matrix multiplication:

$$\mathbf{I} = \boldsymbol{\tau} \cdot \mathbf{E}. \quad (6)$$

A specular layer in this notation appears as a diagonal matrix, since the outgoing and incoming angles must be the same in that case. The notation and the calculation method are derived and explained in more detail in (Klems 1994B) and (Klems and Warner 1995), where technical matters such as the distinction between front and back bi-directional properties and the numbering conventions for layers are discussed. The key relation developed in those papers is a composition equation for computing the property matrices of a system of n+1 layers that is formed by adding a known layer to a (known) subsystem of n layers, as illustrated in Figure 1:

$$\mathbf{T}_{n+1} = \boldsymbol{\tau}_{n+1} \cdot \boldsymbol{\Lambda} \cdot \left(\mathbf{1} - \mathbf{R}_n \cdot \boldsymbol{\Lambda} \cdot \boldsymbol{\rho}_{n+1} \cdot \boldsymbol{\Lambda}\right)^{-1} \cdot \mathbf{T}_n, \quad (7)$$

where the Greek letters $\boldsymbol{\tau}_{n+1}$ and $\boldsymbol{\rho}_{n+1}$ denote the additional transmittance and reflectance matrices, $\mathbf{T}_{n+1}$ denotes the transmittance matrix of the (n+1)-layer system including layer n+1, and $\mathbf{T}_n$ and $\mathbf{R}_n$ denote the transmittance and reflectance matrices of the n-layer subsystem to which layer n+1 is added. Since the n-layer subsystem is entirely arbitrary equation 7 is a recursion relation that allows one to build up a system of any number of layers by repeated application of the equation beginning with n=1 (a "subsystem" composed of a single layer). Analogous equations for reflectance and prescriptions for computing the layer absorptances of an arbitrary system are developed in (Klems 1994B) and (Klems and Warner 1995).

There is nothing mysterious about these mathematical manipulations. Many standard software packages exist to carry out matrix calculations. The calculations for (Klems and Warner 1992), which treated a diffusing shade under simplified assumptions and needed only 7 X 7 matrices, were done using a standard spreadsheet program. For the larger vectors and matrices necessary to deal with two-dimensional input and output angle specifications the manipulations and bookkeeping become tedious and confusing, and special-purpose software (utilizing standardized calculation packages, such as matrix inversion) was written to carry out the calculations. But this was merely for convenience, not because the calculation is in any way specialized or esoteric.

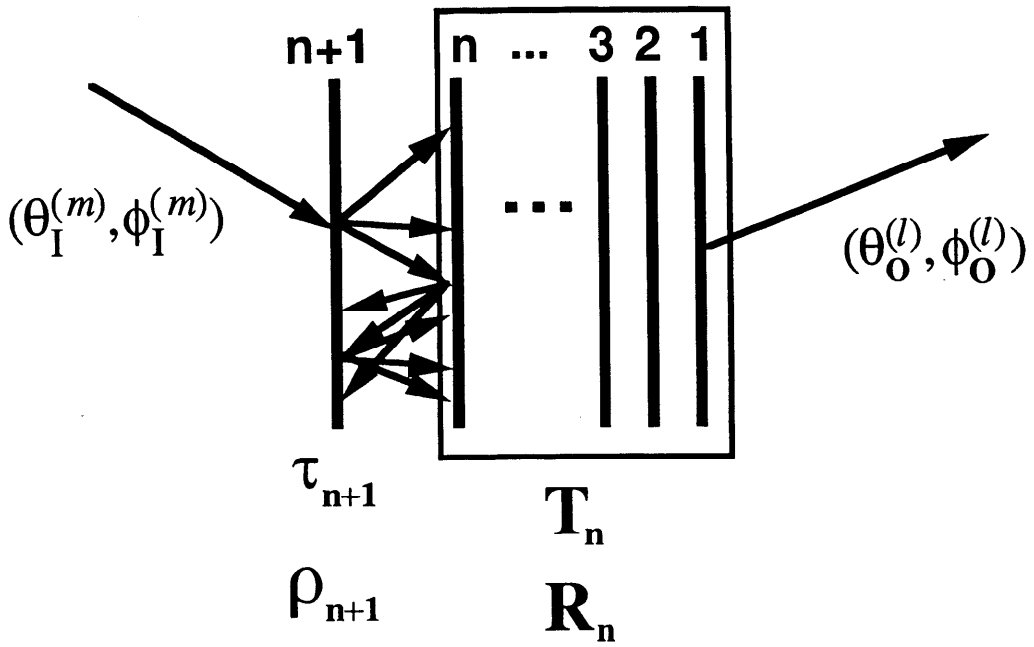

Fig 1. Schematic representation of the addition of an additional layer to an existing system of n layers to form an (n+1)-layer system. The layer property matrices indicated are transmission t and reflectance r and the subsystem transmittance and reflectance matrices are denoted T and R, respectively. The diagram illustrates that the (n+1)layer system transmittance matrix element connecting an incident ray $(\theta_I^{(m)}, \phi_I^{(m)})$ with an outgoing ray $(\theta_O^{(l)}, \phi_O^{(l)})$ must include contributions from rays multiply reflected at all angles between the back side of the layer and the front side of the subsystem.

Measurement of Layer Bi-directional Optical Properties

To make layer bi-directional solar-optical properties we converted the LBL "automated scanner" into a large-sample, automated gonio-radiometer/photometer , shown in Figures 2 and 3. In this apparatus a calibrated detector measures the outgoing radiation at a large number of angular positions distributed over either the front or rear outgoing hemisphere, and this measurement is repeated for all combinations of incident angles that it is necessary to sample, depending on the inherent symmetry of the layer under test. Bi-directional transmittance and reflectance are determined from these measurements and the measured incident irradiance. Radiometric (350-2200 nm) and photometric data are recorded simultaneously. This apparatus has been variously denoted a "scanning radiometer", an "automated scanner" and a "bi-directional scanner", depending on which of its features was being emphasized; for brevity we refer to it here as the "scanner". Details of the scanner operation and the measurement method are contained in (Klems and Warner 1995).

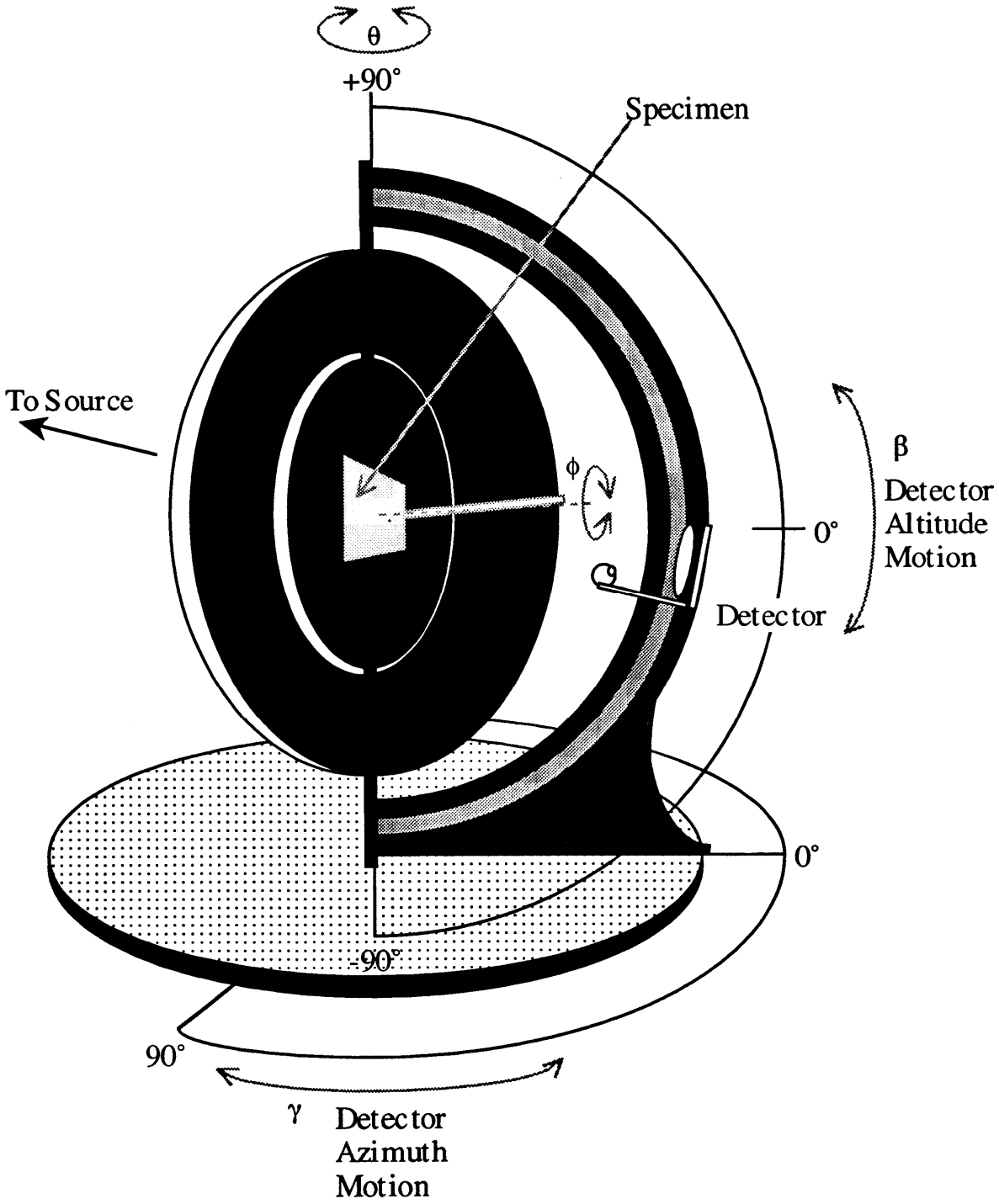

Fig 2. A Schematic Drawing of the Scanning Radiometer. The apparatus consists of a fixed source and a sample mounted on a plane that rotates about a fixed vertical axis relative to the source, to produce a given incident angle, θ. The sample also rotates about an axis perpendicular to this plane to produce the incident azimuthal angle, ϕ. The detector is mounted on a semicircular arm that rotates through the probe azimuth angle, γ, about a vertical axis through the center of the sample. The detector moves up and down over this semicircular arm to vary the probe altitude angle, β, producing an angular coverage over the entire outgoing hemisphere relative to the sample.

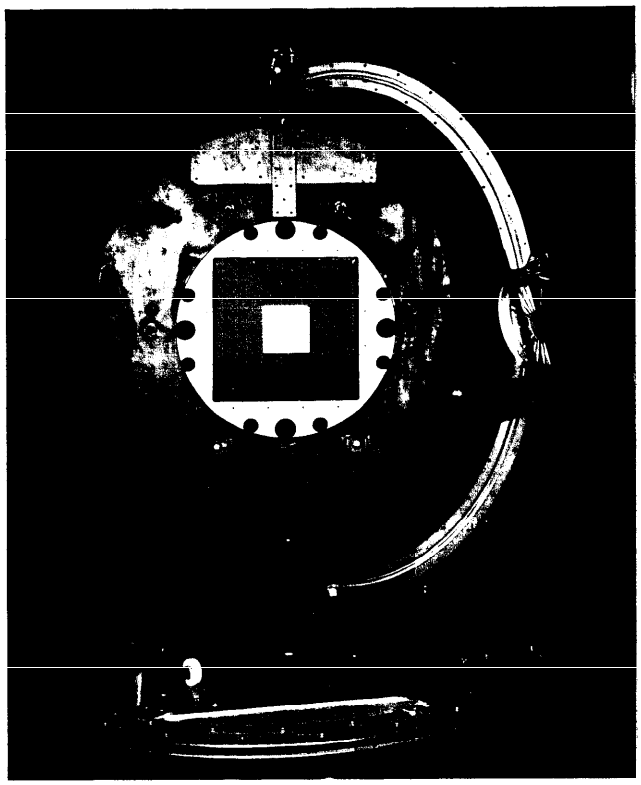

CBB 900-8295

Fig. 3 A photograph of the Scanning Gonio-Radiometer/Photometer ("Scanner"). The detector arm is in the forward-hemisphere-scanning configuration used to measure bidirectional reflectance.

The scanner calibration was checked by making bi-directional measurements on a 7.5 in. square Spectralon® lambertian reflector of known (approximately 98%) hemispherical reflectance, uniform with wavelength over the 350-2200 nm region. The bi-directional measurements were analyzed with our software to produce the directional-hemispherical reflectance, which is shown in Figure 4. The measured hemispherical reflectances are consistent within their experimental error with the 98% reflectance of the calibration sample. Measurements become very inaccurate (±40%) at the largest incident angle (75°) but are still reasonably accurate (±10%) at 60° incidence. Part of the uncertainty at 75° incidence comes from surround reflectance and affects only reflectance measurements; however, uncertainties in the geometric acceptance at this angle remain substantial.

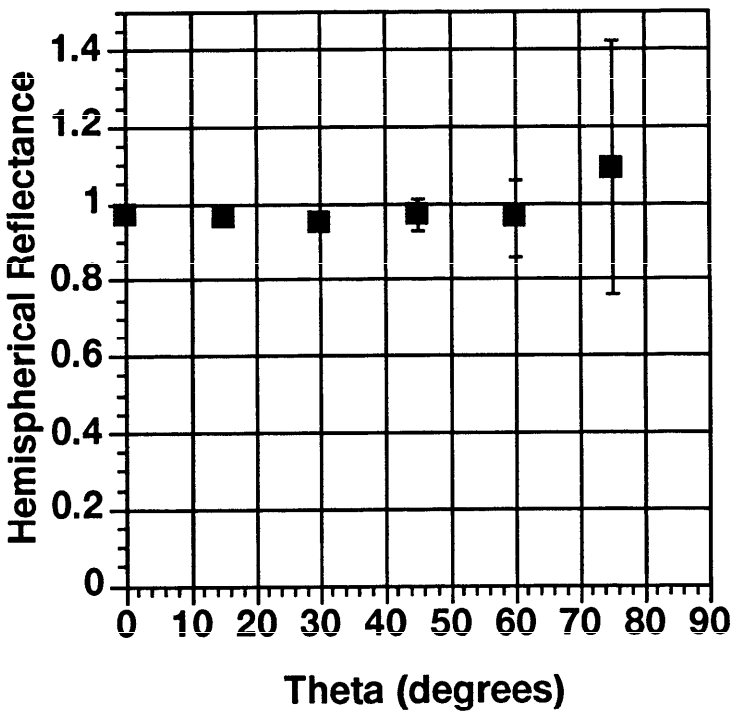

Fig. 4 Measured Hemispherical Reflectance of Spectralon® Calibration Sample. Data measured with the radiometric sensor was used in the determination.

We next proceeded to measure the shading devices to be included in the layer properties data base. These devices are listed in Table 1. In the current data base, a venetian blind with its slats adjusted to different tilt angles is considered a set of distinct devices, as indicated in the table. From this list we selected out two devices to be used in the proof-of-concept study. These were the light translucent shade, described by its manufacturer as "white, light-filtering" and the light-colored venetian blind, which appeared to be a color close to off-white, but was described by its manufacturer as "buff". The measurements on the latter for a 45° slat tilt were used. These two candidates were chosen because they were taken to represent the extremes of difficulty for the application of the layer method. Measurements on the white translucent shade were utilized to determine

the directional-hemispherical properties shown in Figure 5. Derived by integrating measurements of the complete outgoing distribution and determining absorption from the measured transmittance and reflectance, these measurements confirm the assumptions of (Klems and Warner 1992) on this system, which assumed diffuse behavior at large outgoing angles. These measurements show small differences between the photometric and radiometric properties of the shade; however, the radiometric signal is quite small and we consider the differences to be unreliable because of potential uncertainties in background subtraction and thermal drift which are not well known yet and are not included in the estimated errors. This interpretation of the results is strengthened by the fact that the calculated absorptances (which are calculated from the hemispherical transmittance and reflectances) are negative in some instances, although in each of these, consistent with zero within our estimated error.

Table 1. Devices Measured with the Scanning Radiometer

Device	Color	Type or Slat Tilt	Comments
Drape,	Light,	Open Weave	separate specular measurement
Drape,	Light,	Closed Weave	
Drape,	Dark,	Open Weave	separate specular measurement
Drape,	Dark,	Closed Weave	
Venetian Blind,	Light,	0° (open)	separate specular measurement
Venetian Blind,	Light,	45° tilt	separate specular measurement
Venetian Blind,	Light,	90° (closed)	
Roller Shade,	Light,	Translucent	
Roller Shade,	Dark,	Translucent	
Roller Shade,	Light,	Opaque	
Roller Shade,	Dark,	Opaque	
Woven Fabric Screen,	Light		separate specular measurement
Woven Fabric Screen,	Dark		separate specular measurement

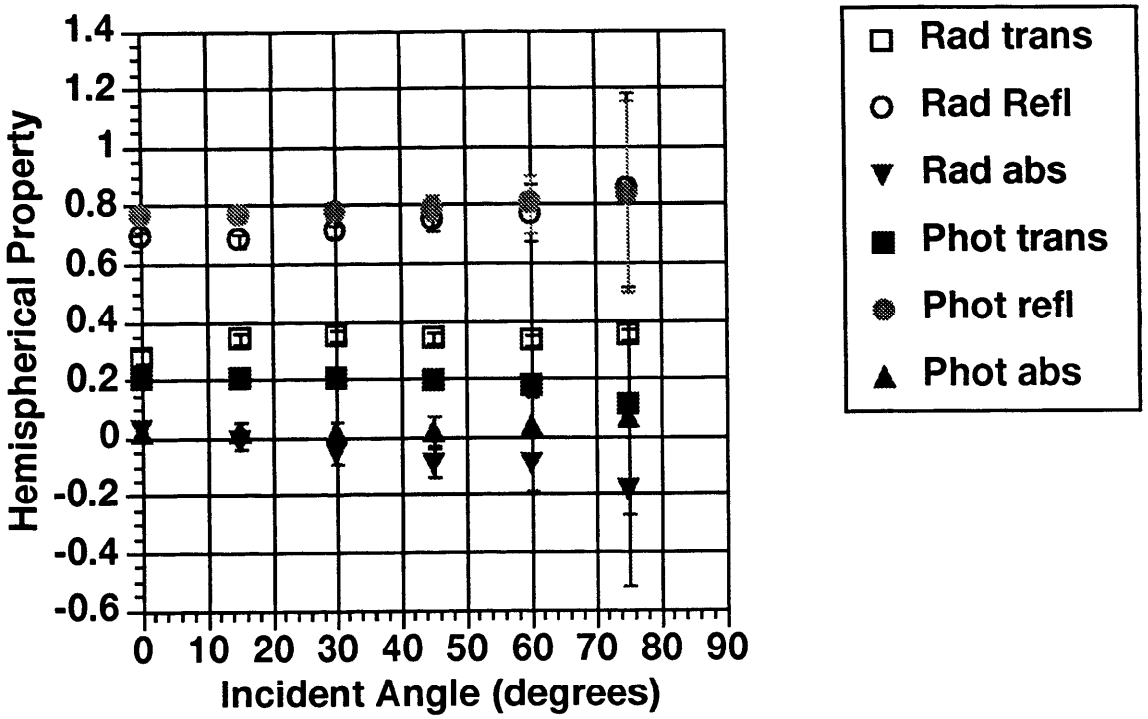

Fig. 5 Measured Directional-Hemispherical Properties of a Commercially Purchased Translucent White Shade.

Figure 6 illustrates the transmittance properties of the light-buff-colored venetian blind. This figure is drawn from a set of measurements made on the blind with the slats at a 45° tilt; data was also accumulated for the slats fully closed and fully open (horizontal). Each set of measurements included bi-directional measurements over the full range of incident and outgoing directions for both reflection and transmission, front and back incidence. Where possible, symmetries were utilized to reduce the number of measurements that needed to be made, e.g., since the blinds are right-left symmetric, it was only necessary to measure over a range of 180° in the incident azimuth, rather than 360°. The full outgoing hemisphere was measured for each incident condition, as described above.

In Figure 6 the upper plot (A) presents the directional-hemispherical transmittance as a function of incident direction, while the lower plot (B) gives the transmittance distribution function τ as a function of the outgoing angles in the scanner measurement coordinate system. Each point in the plot (A) results from integrating over a plot such as the one shown in (B). The particular incident direction corresponding to plot (B) is indicated by the arrow in (A), and corresponds to the measurement configuration shown in Figure 6. If we visualize the venetian blind as mounted in a window in the xy plane with the yz plane horizontal and the zx plane vertical and perpendicular to the window, then the figure corresponds to a physical situation in which the sun is at an altitude of 45° and in the plane perpendicular to the window. The angle β then runs along the slats, while γ is the vertical angle of the transmitted radiation, with negative γ denoting downward-going radiation.

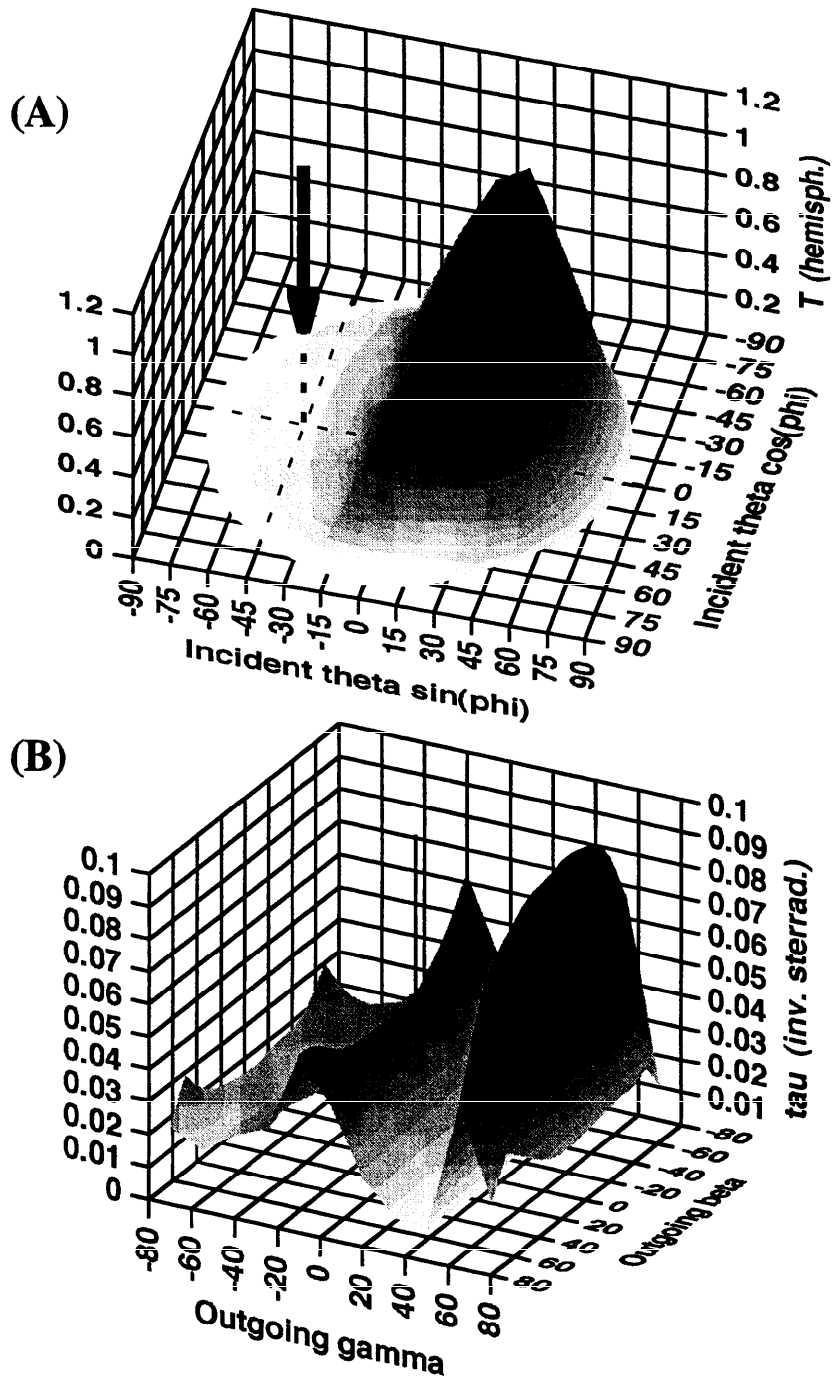

Fig. 6 Transmittance Distributions for a Venetian Blind, Buff, Slat Tilt 45° (dn). (A) Directional-hemispherical front transmittance. The definition of coordinates makes the independent variable plane effectively a polar plot in which θ (in degrees) is the radius and ϕ is the azimuthal angle (measured counterclockwise from the positive x axis). The indicated incident direction has θ=45° and ϕ=180°. **(B) Outgoing transmittance distribution for the single incident direction indicated in (A).**

The strongly asymmetric character of 6A is thus understandable as the result of the downward blind tilt, which excludes the direct sun but is highly transmitting for upward-going radiation reflected from the ground. The outgoing transmittance distribution in 6B thus shows a minimum at the direct sun angle (γ=-45°), a broad ridge at around γ=0, which is radiation twice diffusely reflected from the blind slats, and a higher broad ridge at large positive γ, which is radiation once diffusely reflected from the front side of the blind.

We see from this example the large amount of information necessary to characterize a system as complex as a venetian blind at a single blind tilt. To put this into perspective, a sun-following calorimeter measurement, if successful, might take on the order of half a day, and would give a single point in 6A. On the scanner this measurement takes around 20 minutes, yields around one thousand data points, and enables us to construct 6B in addition to the point in 6A. In either case, in order to characterize accurately the blind heat gain (for a given slat angle) including beam, diffuse and ground-reflected radiation one would need all of the information in 6A, which contains some 78 directional-hemispherical measurements, a lengthy measurement (some 5 days of round-the-clock measurement) with the scanner, but a much more arduous one (a minimum of 39 days) with a calorimeter. The additional detail of 6B provided by the scanner measurement is the information that allows one to carry out a layer calculation, as opposed to making separate measurements for each fenestration combination containing the blind. This means that the 5 days of scanner measurement would provide the information necessary to characterize the venetian blind in all combinations with specular glazing layers. The 39-day calorimeter measurement would need to be repeated for each combination.

Measurement of Inward-Flowing Fraction

The inward-flowing fractions N_i of the absorbed solar energy are the only inherently calorimetric quantities in the determination of the solar heat gain coefficient. In principle they depend on the temperatures of the layers and their surroundings, air temperatures, and air motion. In previous discussions in the literature, they have variously been treated as constants(Yellott 1966) or evaluated theoretically using an idealized heat transfer model.(Farber, Smith et al. 1963) The physical processes that produce the N_i are both understandable and complex. Solar energy absorbed in a particular layer of a fenestration system will divide into inward and outward heat flow in proportion to the ease with which it can flow in the two directions under the prevailing conditions. But this depends on the temperature of the layer in question, of the adjacent layers and of the adjacent air; in addition, the pattern and velocity of adjacent air flow may have an effect, and all of these may depend on the level of solar irradiation. For the outer fenestration layer, wind and exterior air and radiative temperatures would be expected to be important.

For all of these reasons, it was considered important to measure N_i under realistic indoor and outdoor conditions for the proof-of-concept study. Evaluating the extent to which they vary with external weather conditions was an important part of defining the method. Clearly, if the N_i showed a high degree of variability, providing a representative set of values for solar heat gain calculations would be a much more difficult task than if the variability were low.

We performed these inward-flowing fraction measurements using the Mobile Window Thermal Test (MoWiTT) Facility(Klems, Selkowitz et al. 1982) in Reno, NV. This facility consists of two side-by-side room-sized guarded calorimeters. To measure the value of N_i for a layer in a particular fenestration system, identical fenestration systems were mounted in the two calorimeters, with provision made to electrically heat the selected layer in one of the fenestrations. Electrical heat applied to that layer would simulate a small increase in solar absorptance, and if a fraction N_i of the applied power, P, flowed inward, then the net heat flowing through the fenestration would increase by an amount $N_i \cdot P$. Since the calorimeter accurately measures the net heat flow and P is also known, varying P and measuring the resulting change in net heat flow gave a direct measurement of N_i. In this measurement, the companion calorimeter with the unheated layer was used as a control.

The experimental design focused on determining the in-situ values of the inward-flowing fraction, and this meant that the heating power applied to the layer must be a small perturbation to the important variables in the system. The heat was applied in ways that affected the surface geometry and optical properties as little as possible. For metallic venetian blinds electric current was applied at the ends of the blind, with each blind slat itself acting as a heating element. For non-metallic blinds, a thin heating wire was applied to the underside of each blind slat. Non-metallic shades were treated by cementing a layer of the appropriate shading material on each side of a metallic layer, which was heated. This did change the optical transmission somewhat, but we judged this to have little effect on the inward-flowing fraction. We took the key non-geometric variable to be the layer temperature. To keep the change in layer temperature small meant limiting the amount of the applied power, P; however, it was necessary to have a reasonable value for P to produce a detectable signal in the calorimeter. After some preliminary study we settled on a nominal value for P in the range 30-50W. This produced an increase in the layer temperature of a few degrees Celsius. It was observed that a venetian blind in the MoWiTT cycled over a temperature range on the order of 40° C between day and night under summer conditions. From this it was clear that if there were a temperature dependence in the inward-flowing fraction, the small temperature rise due to the applied layer power would not mask the change between day and night. The sole exception to this procedure was the case of exterior venetian blinds, where the inward-flowing fraction was so small that a much higher applied power was necessary to produce a detectable signal in the calorimeters.

At the outset, the inward-flowing fraction was obtained by comparing the difference between apparent net heat flows through the fenestration in the two calorimeters, one with a heated layer and the other without applied heating. Comparing this difference with the applied layer power turned on to the difference with the power off (when it should have been zero) gave the amount of the applied power that flowed inward from the heated layer, and the inward-flowing fraction was directly obtainable from that. This method was used to produce initial results. By selecting data only from the afternoon, as compared with data averaged over the full 24-hour period, we were able to determine that, contrary to expectation, there was not a strong dependence of the inward-flowing fraction on layer temperature.

This method of analysis was subsequently discarded as not sufficiently accurate and reproducible. For many shading systems, particularly venetian blinds, the differences between units were sufficiently large that it did not prove possible to mount different units in the two calorimeters and have the net heat flows be the same for no applied layer power. Initially, it was assumed that the problem was due to adjustment of the blind angles, and considerable effort was spent trying to adjust one or the other blind angle to achieve equal net heat flow. However, we observed that even when a good balance was achieved at the outset, subsequent P=0 measurements under different sky conditions would not show equal net heat flows in the two calorimeters. We finally concluded that variations in stiffness, curvature and position among the slats of the two blinds resulted in two units with intrinsically different transmissions. Although the two devices could be balanced under a given set of sky conditions by small changes in slat angle, this did not make the transmissions identical, but rather used changes in beam transmission to offset differences in diffuse transmission. As soon as the sun angle or the direct-to-diffuse ratio changed, the balance was upset.

In the final analysis we used a method that did not require comparisons between physically distinct shading systems. The measured net heat flow, W(t), through the fenestration was compared with a theoretical prediction given by

$$W_{TH}(t) = (UA)\cdot\left[T_O(t) - T_I(t)\right] + B(t)\cdot I_S(t) + N_i \cdot P \qquad (3.1)$$

where $T_O(t)$, $T_I(t)$, and $I_S(t)$ are the measured values of the outdoor air temperature, indoor air temperature, and incident vertical solar intensity, respectively, at the time t and the subscript i denotes the heated layer, while (UA), $B(t)$, and N_i are parameters that were determined by a least-square fit to the data. An example of a simplified version of the fitting procedure (in which B was assumed to be a single constant) is shown in Figure 7. In the final analysis, the parameter $B(t)$, which is the effective solar heat gain coefficient multiplied by the applicable area, was defined to be time-dependent as follows:

$$B(t) = \begin{cases} B_1 & \text{for no direct sun on window} \\ B_2 + B_3 \cdot \cos(\theta(t)) & \text{for direct sun on window} \end{cases}, \qquad (3.1a)$$

where B_1, B_2, and B_3 are constants, while $\theta(t)$ is the solar incident angle relative to the normal to the plane of the window at time t. In the fitting process, (UA) and B(t) were fit using only that portion of the data for which the layer power was off (P=0), and during this fit (UA) was adjusted only between the hours of midnight and sunrise. The typical measurement of an inward-flowing fraction consisted of installing a given window system in both MoWiTT calorimeters with provision to heat a particular layer of the fenestration in one of the two calorimeter rooms (Chamber B). After both calorimeters were closed and allowed to come to equilibrium, data-taking consisted of several days' to a week's measurement with P=0, approximately the same time period with P set to a constant 30-50W (or more for exterior venetian blinds), followed by another several-day period with the applied layer power off. The layer inward-flowing fraction N_i was determined by fitting the days for which the power was turned on, and during this fit the other parameters were held fixed at the values determined from the days with the power off.

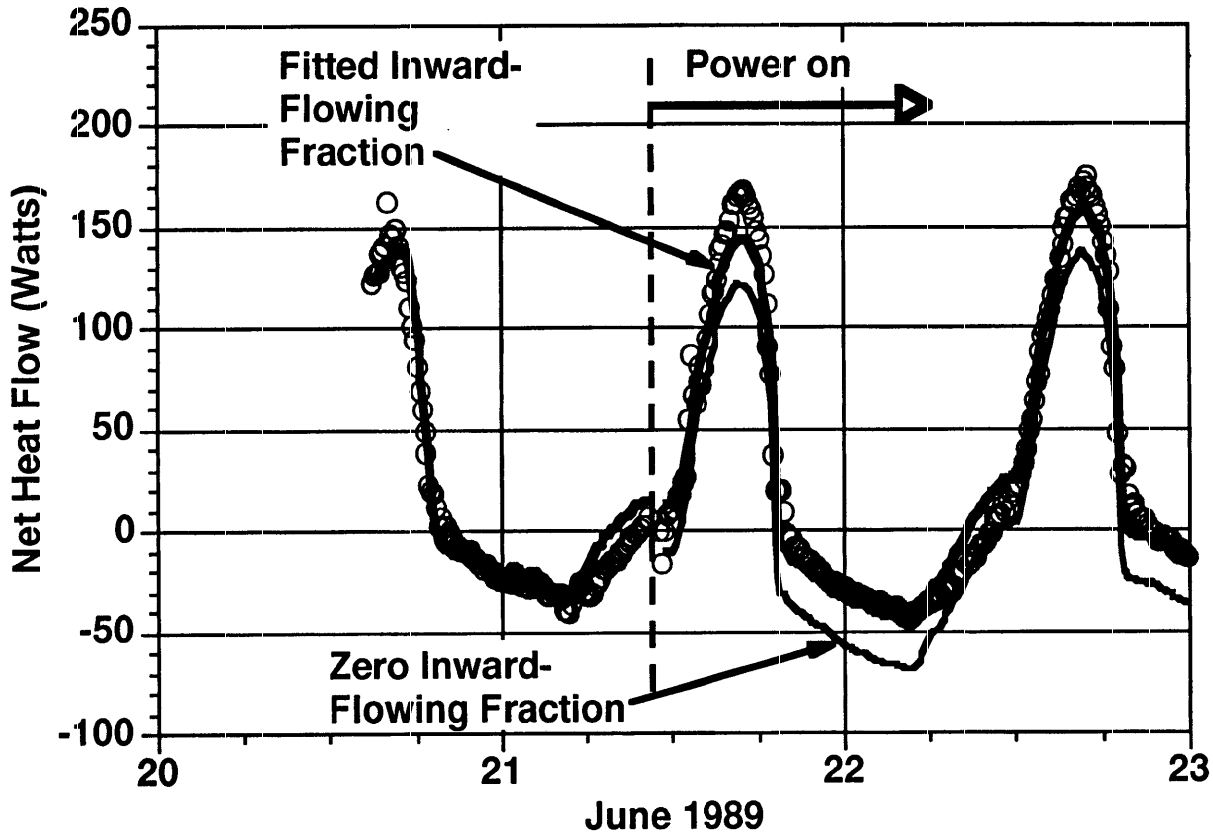

Fig. 7 Determination of N_i for an Interior Shade. The MoWiTT measurement of the apparent window net heat flow is plotted (open circles) together with the calculated curve given by Equation (3.1) for the fitted value of N_i (heavy curve). Comparison with the same equation assuming $N_i = 0$ (light curve) gives a measure of the significance of the determination. The two curves coincide before the power heating the blind was turned on. This figure illustrates a fit using a single constant value of B, before the additional sophistication of Equation (3.1a). The fact that the model of Equation (3.1) does not accurately fit the measured points in the morning or near the solar intensity peak illustrates the limitations of the assumption of a constant value of F.

Table 2 Measured Layer Inward-Flowing Fractions, N_i, for Geometrically Prototypical Systems

System	Bind angle below horiz.	Inner Shading Layer	Inner Glass	Between-Pane Shading	Outer Glass	Exterior Shading Layer
Single Glazing with Interior Shade		0.80±0.08			0.08±0.06	
Single Glazing with Interior Venetian Blind	-45°	0.69±0.05			0.24±0.09	
	30°	0.83±0.08			0.21±0.07	
	Clsd	0.72±0.07			0.14±0.05	
Single Glazing with Exterior Venetian Blind	45°				0.46±0.12	0.04±0.01
Double Glazing with Interior Shade		0.85±0.10	0.52±0.12		0.28±0.06	
Double Glazing with Interior Venetian Blind	45°	0.86±0.06	0.69±0.14		0.21±0.09	
Double Glazing with Between-Pane Blind	45°*		0.69±0.14	0.45±0.06	0.34±0.10	
	-45°		0.76±0.10	0.40±0.07	0.27±0.14	
Low-E Double Glazing with Between-Pane Blind	35°		0.46±0.12	0.38±0.05	0.32±0.11	
Double Glazing with Exterior Venetian Blind	45°		0.73±0.13		0.28±0.12	0.03±0.02

* Blind measurement was made at 30° rather than 45°.

The values of the layer inward-flowing fractions determined by this method are shown in Table 2. The principal contributor to the quoted errors in the table was the estimated systematic uncertainty in the absolute net heat flow measurement of the calorimeter, which was typically 2-4W during these tests. The uncertainty arising from the fitting process, estimated by standard statistical techniques, was much smaller. In all cases the quoted error corresponds to one standard deviation. The RMS value of the deviation between the measured and predicted net heat flow was in the range 10-30W.

The angular dependence used for the effective solar heat gain coefficient in equation 3.1a was selected as the simplest form that provided stable fits to the data. We initially tried a theoretical form that used a constant direct-sun value for B. We found that this produced a curve that did not peak as sharply during the daytime as did our measured values of W(t). This resulted in a curve that fit partly cloudy days better than very clear days, and if the power-on and power-off measurement periods differed significantly in this respect, the resulting value of N_i would be biased. For four cases where we had made two separate measurements of the same fenestration system layer at different times, we obtained values of N_i that were not consistent within experimental uncertainties. With the angular dependence of equation 3.1a, these repeated measurements each produced consistent values of N_i.

Using this method of data analysis we tested for temperature dependence by repeating the above fitting process while allowing N_i to have a different value, $(N_i)_{PM}$, in the afternoon (during which, for our west-facing tests, the window was in direct sunlight and all parts of the glazing system were at substantially higher temperature) from that of the night and morning, $(N_i)_{AM}$. This test produced no significant evidence for temperature dependence in N_i. There was a tendency for the difference $(N_i)_{PM} - (N_i)_{AM}$ to be positive, but on the average the magnitude of this difference was comparable to the experimental error. For the five systems on which we had made repeated measurements at different times we computed the mean and standard deviation of $\Delta N_i = (N_i)_{PM} - (N_i)_{AM}$ for each pair of repeated measurements. We found that the mean difference is never larger than the standard deviation, which is a measure of the consistency of results obtained on separate measurements of the same system. From this we conclude that the temperature dependence of N_i, if any, is not large compared to the experimental uncertainty. It is therefore sufficient to treat the N_i as constants within the measurement uncertainties in Table 2.

This conclusion must be regarded as encouraging, but preliminary because of the lack of a plausible model of temperature dependent inward-flowing fractions to test against the data. In this research all of the issues regarding inward-flowing fraction measurement procedure, tests for temperature and weather dependence, and methods of extracting information from the measurements had to be addressed simultaneously, and not surprisingly we do not regard our tests as definitive on this issue. It is possible that either improved analysis or more accurate and controlled tests will reveal behavior of the inward-flowing fractions that was masked by measurement uncertainties or analysis artifacts in this treatment. On the other hand, small variances in the N_i with ambient conditions will not greatly affect the SHGC calculated from equation 1.

Comparison of the Layer Calculation with MoWiTT Measurements

MoWiTT Measurement of Solar Heat Gain Coefficients

The MoWiTT Facility also provides a calorimetric measurement of the solar heat gain. In equation (3) above the constants B_i determined in the fit provide a simplified model of the solar heat gain coefficient. A more sophisticated model was not needed for the N_i determinations because the solar gain characteristics of the modified prototypic systems in Chamber B used to measure the inward-flowing fractions are of no intrinsic interest.

However, the baseline comparison systems measured in Chamber A were in some cases unaltered fenestration systems utilizing the same elements studied with the scanner. Subsequent to the above analysis, this data was analyzed in more detail using the following model:

$$W(t) = A \cdot \left[T_o(t) - T_i(t)\right] + B_D \cdot g_0(t) \cdot I_D(t) + \left[\sum_{n=1}^{6} B_n \cdot g_n(t)\right] \cdot I_B(t) \cdot \cos(\theta(t)), \quad (4.1)$$

where A, B_D and B_n are fitted constants and the functions g_0 and g_n are defined as

$$g_0(t) = \begin{cases} 1 & \text{if the sun is up at time } t \\ 0 & \text{otherwise} \end{cases}$$

$$g_n(t) = \begin{cases} 1 & \text{if } t \text{ is within hour } n \\ 0 & \text{otherwise} \end{cases} \quad (4.2)$$

The intensity of the beam radiation I_B is determined from the pyrheliometer included in the MoWiTT instrumentation. This is also used to calculate the diffuse part, I_D, of the vertical-surface solar intensity at the window. The angle $\theta(t)$ is of course the instantaneous solar incident angle. The n hours were selected as those for which direct sun illuminated the window, afternoon hours in most cases, since the orientation was west-facing. When there were not six hours of daylight, terms were dropped from the sum and the corresponding B values ignored in the fitting.

This fitting procedure yielded for the B_n hourly average values of $\langle F(\theta,\phi)\rangle \cdot A_G$, where A_G is the glazed area of the fenestration. By separately averaging the solar angles over the same hourly intervals, we could associate the B_n with the corresponding average sun angles. Since the sun angles may change on the order of 15° per hour, this procedure gave us an angular resolution comparable to that of the scanner measurements.

For the case of the buff venetian blind (for which scanner measurements are described above) mounted as an interior blind on a wood-frame, double-glazed window (2.5 mm clear glass each pane), the derived beam solar heat gain coefficients are plotted in Figure 8 as a function of solar incident angle for three separate measurements made at widely separated times and during various months from April to November. The angular

dependence of the solar heat gain coefficient is apparent from this data. The separated measurements agree with one another reasonably well, even though the solar azimuths of data points with the same incident angle may be substantially different. This point will be discussed further below. Differences between measurements may also reflect the difficulty of setting the blind slats at a precisely reproducible tilt angle in the field. For points at both extremely high and extremely low incidence angles the hourly SHGC determinations are untrustworthy and were not included in the plot, and the largest-angle points included have substantial experimental uncertainties. The high angles occurred just after solar noon when the sun begins to be incident on the west-facing facade; these conditions are particularly sensitive to window reveal, exact placement of the blind relative to the window frame, and other idiosyncrasies of the experiment. Low angles, on the other hand, occurred near local sunset (when the sun disappears behind the mountains) and correspond to low solar intensity. Errors in heat flow measurement, small residual time lags in the chamber, and similar effects were combined with the fitting uncertainty to produce the error bars on the points. In addition, the particular fit method used may produce underestimates of the true uncertainty, since certain correlations between the fitted parameters were disallowed in order to avoid predictable experimental problems. For example, hours when there were direct sun were not allowed to contribute to the fitting of the diffuse constant.

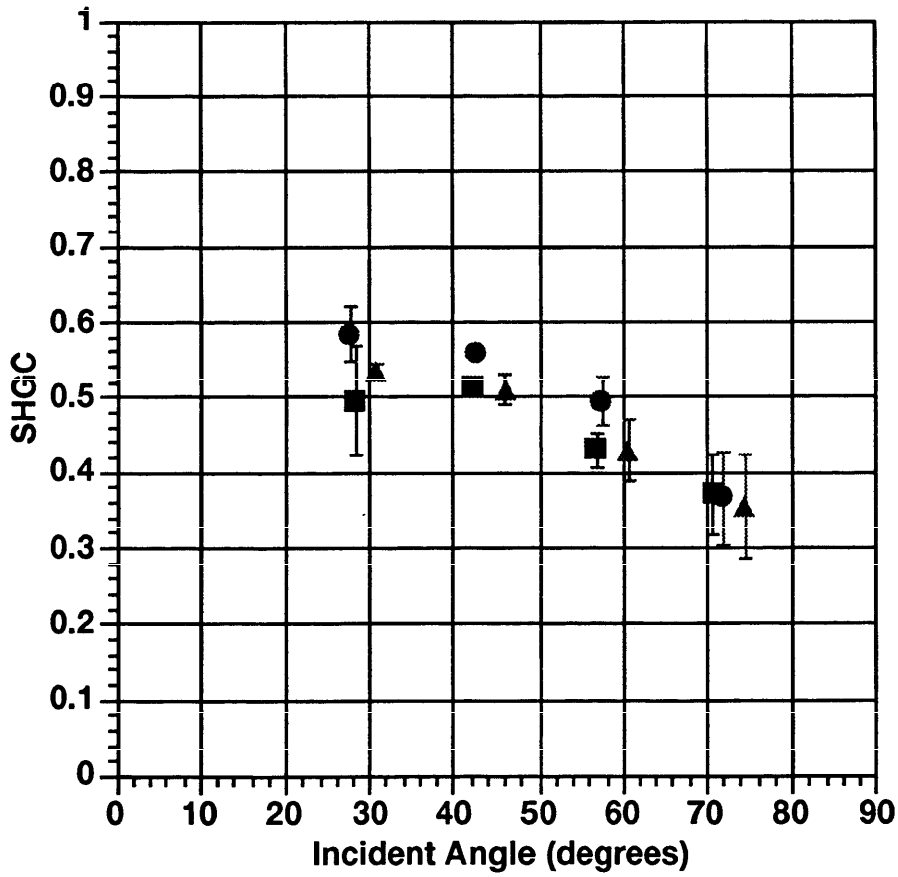

Fig. 8 Angle-Dependent Solar Heat Gain Coefficients for the Venetian Blind Derived from MoWiTT Data. Squares: Oct., 1988 measurement period; triangles: Aug., 1989 measurement period; solid circles: Sept., 1991 measurement period.

Comparison of the Layer Calculation with MoWiTT Measurements

The scanner measurements of $\tau^f(\theta_o,\phi_o;\theta_i,\phi_i)$, ρ^f, τ^b and ρ^b discussed above for the buff venetian blind with 45° slat tilt together with published (Rubin 1985) properties of clear glazing were utilized in the layer calculation method described above to produce the directional-hemispherical transmittance and system directional layer absorptances for double glazing with interior blind. The layer calculations were carried out and were in turn combined with the results for N_i from Table 2 using equation 1 to produce the beam solar heat gain coefficient, $F(\theta,\phi)$. The angle ϕ, which was defined in (Klems 1994A) for the layer coordinate systems, is inconvenient when discussing sun angles. We use instead the angle ψ, where $\psi=\phi-180°$. The angle θ retains its identity as the angle of incidence. The relation of these angles to the sun direction is shown in Figure 9. The beam SHGC as a function $F(\theta,\psi)$ of these two angular variables is displayed in Figure 10 for downward-going incident directions.

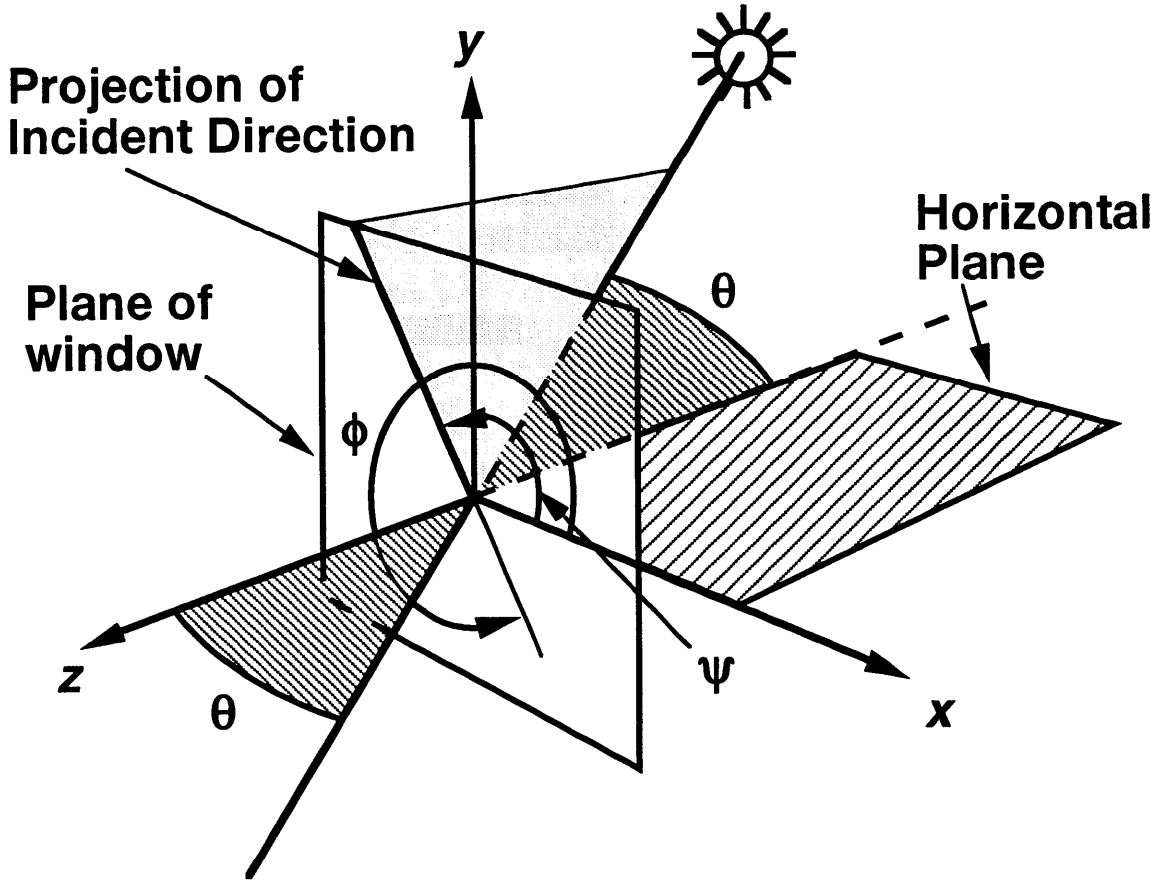

Fig. 9 Relation Between Sun Angles (θ,ψ) and Layer Coordinates (θ,ϕ).

The calculation in Figure 10 is based on the photometric data accumulated by the scanner. A second calculation was also carried out using radiometric (spectrally flat) sensor data. In principle, the latter is preferable; however, in this instance a number of problems made the radiometric data suspect. First, the low transmission of the blind in the forward direction meant a low radiometer signal in that sensor, which because it is a

thermal sensor is much less sensitive than the photometric. For the photometric sensor internal noise is negligible; for the radiometric sensor it was a serious problem. The sensor was also vulnerable to thermal drifts, and we had some indication that there was heating of the sensor and integrating sphere in angular configurations for which there was higher transmittance, and this in turn may have caused thermal drifts that were significant when the detector moved to a region of smaller transmittance. Since we do not expect a great deal of spectral selectivity between the visible and near-infrared regions for this fenestration system, we are inclined to believe the photometric sensor when the two disagree.

In Figure 10 the solar heat gain coefficient is shown only for downward-sloping incident directions ($0 \leq \psi \leq 180^{o}$). Upward-sloping incident directions can occur only for ground-reflected radiation, which is a broad angular distribution because the reflection is diffuse. Ground-reflected radiation will appear as a part of the diffuse component of the incident solar intensity, which at least on clear days is much smaller than the beam contribution. In the following we will be discussing primarily beam radiation. The transmittance for upwardly-sloping incidence does appear as part of the solar heat gain coefficient for downward incidence, but (as can be concluded from visualization), the radiation must first undergo at least two reflections, one from the blind and the other from the pair of glass layers. Since the blind reflectance is non-specular and the reflectance of the glass system is low, the upward-going intensity incident on the blind will be low; hence, small variations in the transmittance for upward-going radiation will not affect the overall system transmittance appreciably. For this reason, we conserved measurement time by deriving the upward-incident front transmittance of the system from the downward-incident back transmittance measurements, which by assuming front-back blind symmetry neglects the effects of slat curvature. We do not expect that appreciable errors are introduced by this assumption.

As can be seen from Figure 10, variation of $F(\theta, \psi)$ is much stronger with θ than with ψ, which made it meaningful to plot the data as in Figure 8. The MoWiTT measurements from which this graph is drawn are listed in Table 3, from which it can be seen that the overall variation in ψ is substantial, however, and a quantitative comparison between the measurement and calculation must take this into account. Figure 11 shows the actual sun path in the appropriate coordinate system for the measurement periods corresponding to the data, superimposed on the contour plot of $F(\theta, \psi)$. The calculated values are hourly averages of F along those contours, corresponding to the hourly SHGC values determined from the data.

In Figure 12 we compare the data and calculations in Table 3. Each set of points must be compared only to its corresponding curve; for example, the 1989 data fits its curve more closely than do either of the other two data sets; the fact that the 1991 curve lies close to the 1988 data and visa versa is an irrelevant by-product of displaying all three data sets on the same plot and should be ignored.

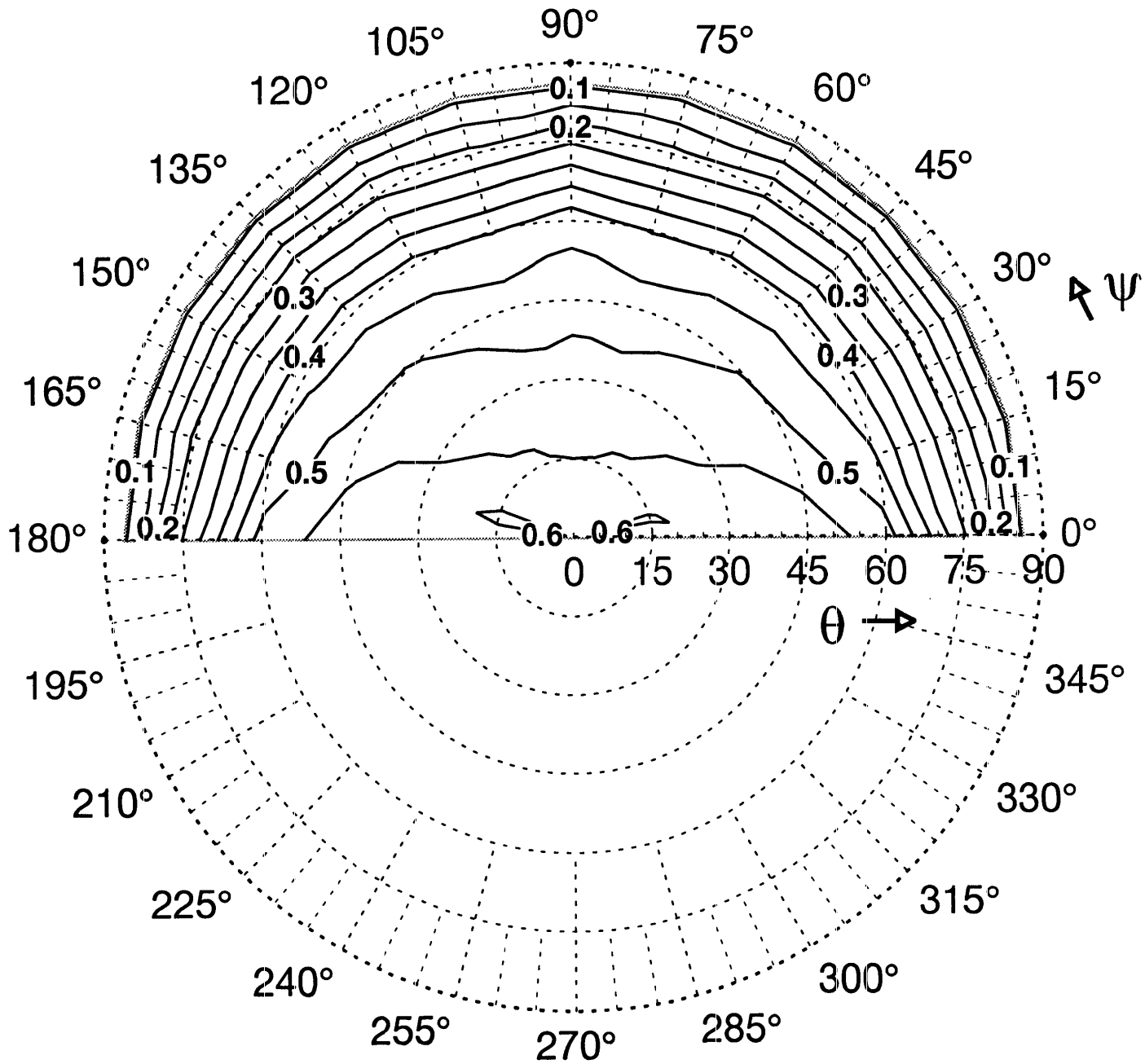

Fig. 10 Calculated Solar Heat Gain Coefficient. Utilizing the layer method, the measured bidirectional photometric properties and inward-flowing fractions were utilized to calculate the directional solar heat gain coeficient (for downward-sloping incident directions), which is displayed here as contours of constant SHGC plotted in a polar plot where the radius is the incident angle, θ, and the azimuth is the incident azimuthal direction, ψ.

Table 3 MoWiTT Measurements and Layer Calculation of the Solar Heat Gain Coefficient for Clear Double Glazing with an Interior Venetian Blind, Slat Angle 45° Down

Measurement Run	Mean Solar Incident Direction		SHGC	
	θ (degrees)	ϕ−180 (degrees)	MoWiTT Measurement	Layer Calculation
Oct, 1988	28.29	159.03	0.49 ± 0.07	0.59
	42.48	149.84	0.51 ± 0.01	0.52
	56.77	145.73	0.43 ± 0.02	0.45
	70.77	143.87	0.37 ± 0.05	0.25
August, 1989	30.90	111.89	0.53 ± 0.01	0.52
	46.07	117.10	0.51 ± 0.02	0.48
	60.58	119.31	0.43 ± 0.04	0.40
	74.47	120.03	0.35 ± 0.07	0.22
Sept, 1991	27.56	132.69	0.58 ± 0.04	0.54
	42.57	131.60	0.56 ± 0.01	0.50
	57.54	131.27	0.49± 0.03	0.43
	71.84	130.94	0.37 ± 0.06	0.27

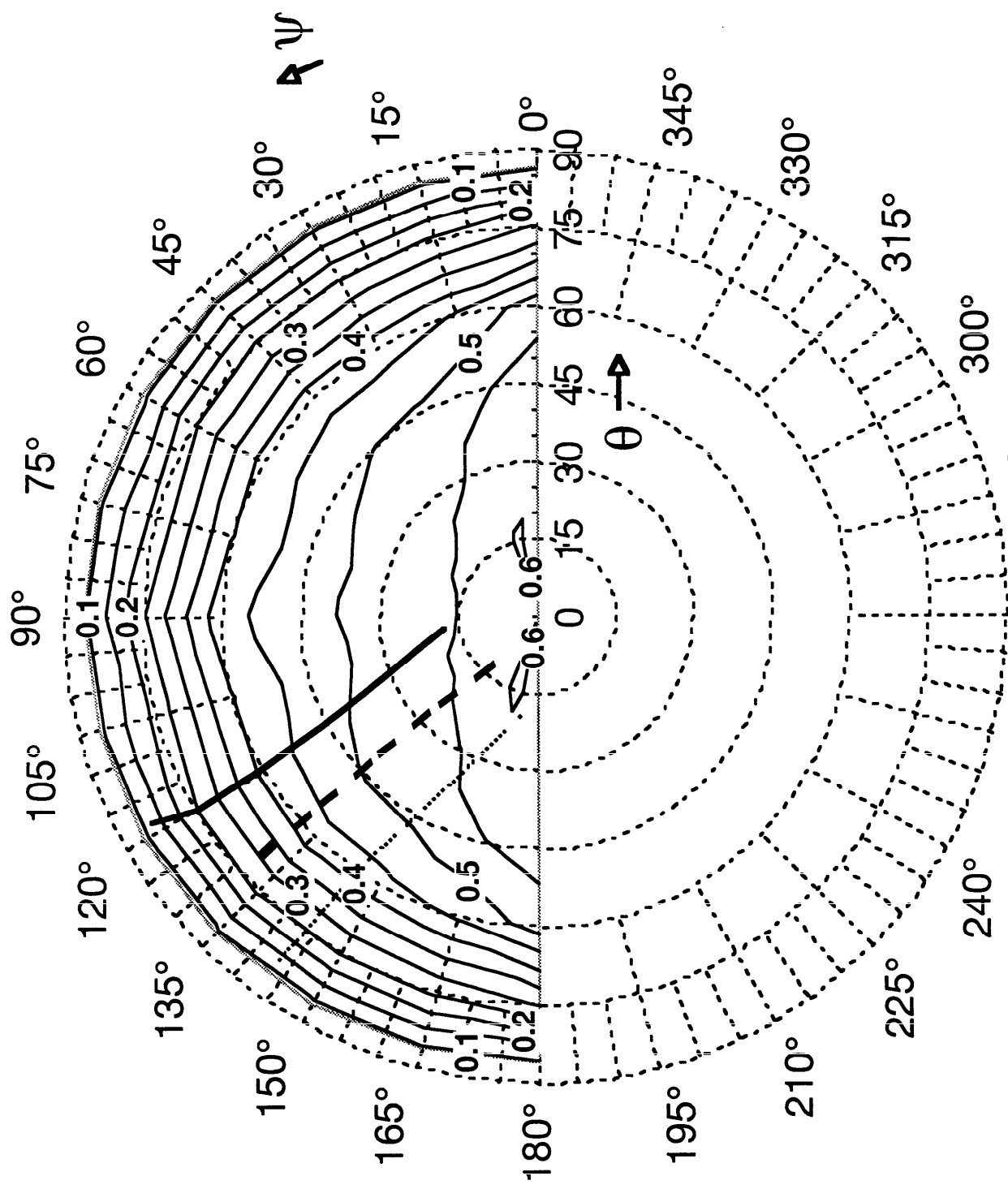

Fig. 11 Averaged Sun Trajectories of the MoWiTT Measurement Periods Compared with Calculated Directional SHGC for the Buff Venetian Blind at a 45° (sun-excluding) Slat Angle. Heavy solid line: Aug., 1989 period; heavy dashed line: Sept., 1991 period; light dotted line: Oct., 1988 period.

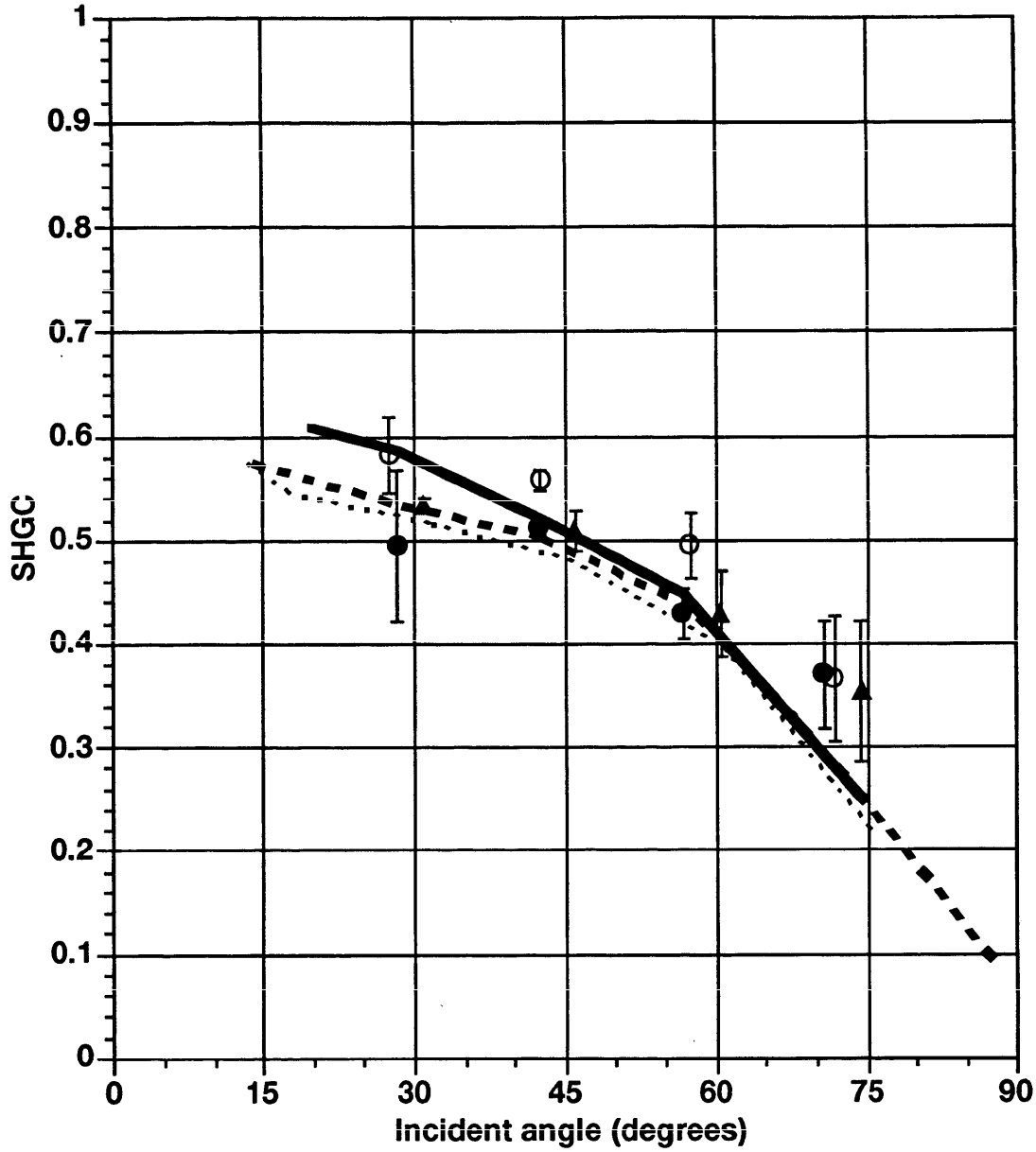

Fig. 12. Comparison of the Layer Calculation of SHGC with the MoWiTT Measurements for Clear Double Glazing with and Interior Venetian Blind. Three sets of measureed points from measurement periods with slightly different sun trajectories are shown with their corresponding curves calculated with the layer method: Oct., 1988: Solid circles and heavy solid line; Aug., 1989: Open circles and heavy dashed line; Sept., 1991: Solid triangles and light dotted line.

Discussion

We consider the layer calculations and the MoWiTT measurements in Figure 12 to be in quite significant agreement. The calculation reproduces the angular trend in the data

quite well, with the normalization of the curve matching to within 10% in all cases of importance, and in one of the data sets matching quite closely indeed. Considering the difficulty of arranging the blind tilt reproducibly in the field (a difficulty exacerbated by other issues that were being investigated simultaneously), one would scarcely expect better agreement. Where there are larger deviations between the points and the curves, one expects poorer reliability in either the calculation or the measurement (or both). This occurs at the end of the curve: the large-angle end with the highest sun angle in each data set may give data of poor quality because of the effects of window reveal and blind edges, which are not dealt with in the calculation. In addition, as discussed in the section on scanner measurements, large errors in the region of 75° incident angle are expectable.

Venetian blinds are expected to be among the most severe tests of the method, and agreement of the angular dependence puts a stringent test on the whole calculation methodology. The system front transmittance and blind layer absorptance in the system have magnitudes that are in some places comparable but have quite different angular shapes. Since the blind inward-flowing fraction is some 86%, both of these make comparable contributions to the solar heat gain coefficient. Matching the MoWiTT angular dependence thus does not come about through the trivial domination of a single physical effect (as is true for transmission in unshaded glazings).

That we were able to extract a reproducible angular-dependent solar heat gain coefficient from the MoWiTT data is in itself a remarkable new achievement. Operating in a fixed orientation for any given test (rather than following the sun), the MoWiTT both represents a realistic window environment and experiences a variety of sun angle conditions. Operating a calorimeter in this mode has been controversial, and the demonstration that detailed angular information can be disaggregated from the data gives an important new option in fenestration system property measurement.

Data Presentation Format

The bi-directional optical property data, representing as they do tabulations of (in the most complicated case) four-dimensional functions, may be of interest for specific partial presentation (for example, in the example plots presented in this report), but is in general too detailed and voluminous to be useful as anything other than an intermediate data library for the use of automated calculations. In this it is analogous to the glazing spectral data bases used by calculation models, such as WINDOW or VISION, for specular glazing SHGC determination. Indeed, there is no difference in principle between the detailed data required by the layer method and the data required by an ordinary U-value calculation. In the latter case, it is true, the detailed and complicated heat transfer correlation information is conveniently summarized by semi-empirical formulas, but once one has moved from simple glazing U-values to overall window U-values, it becomes necessary to include a large amount of information about detailed frame design and geometry in order to produce a result. As U-value treatments extend to more geometrically complex glazing elements, such as skylights and greenhouse windows, it may well be that the heat transfer data will also become less susceptible to formula summaries and require larger system-specific data bases.

There is nothing novel, therefore, in the need for a large and complex intermediate data base.

There is, as was noted at the outset of this project, a formidable combinatorial problem in the area of solar heat gain coefficients, but in terms of data presentation this is also not new. Again, the extension of U-value attention to framed windows and the desire for high accuracy has introduced the combinatorial problem to U-values; the chief difference here is that the potential number of combinations is much larger for shading systems.

The new problem is the sensitivity of the final result to orientation, location and solar position, at least for some complex shading systems. In comparing the calculations with MoWiTT measurements we touched on this problem; here we examine its implications for the presentation of SHGC, e.g., in the Handbook of Fundamentals.

The organization and function of the data base accumulated in the course of this project is outlined in Figure 13. It has a directory tree structure consisting of two arms. The more basic arm is the layer data, which contains the bi-directional layer solar-optical (and photometric) properties. These may come from a variety of sources; in the present instance they are produced either from manufacturer or published data (manufacturer or published data (for specular glazings), or from scanner measurements. They may also be produced theoretically for specific model systems (e.g., perfectly diffusing layer, theoretical model of a venetian blind, etc.). It is also envisioned that in the future they may be produced by detailed calculations from material surface and system geometrical properties, e.g., by monte-carlo ray-tracing.

The second arm consists of systems identified by a unique I.D. 3-digit code built up from the layers by the layer calculation. Entries in this arm are added automatically as calculations of system properties are carried out by the layer calculation program (called TRA). A system has an I.D. code constructed by listing the layer I.D.'s that compose it, from outside to inside. For example, if 999 is the code for a clear 3mm sheet of glass and 060 is the code for a buff venetian blind at a 45° slat angle (in the current organization, different slat tilts are treated as different layers), then the system code 999999060 would define a clear double glazing with interior venetian blind (45° slat tilt), while the code 999060999 would define a clear double glazing with blind between the panes and 060999999 a clear double glazing with exterior blind. A separate calculation, indicated in the figure, combines the optical data files for the system with the appropriate inward-flowing fractions to produce the directional solar heat gain coefficient for the system.

In Figure 14 is a repeat of the contour plot, shown previously, of the polar directional beam SHGC for the double glazing with interior buff venetian blind at a 45° downward slat tilt. Superimposed on the plot are the sun trajectories in this coordinate system for 40 degrees North Latitude. The trajectories are plotted for three orientations of the window and for the days of the summer and winter solstices and the (spring or fall) equinox. Over the course of a day the sun will travel from left to right in the figure along the appropriate trajectory.

It is clear from the figure that for most of the conditions the system will have a solar heat gain coefficient that varies with time. Only for the case of the winter solstice does the

sun trajectory follow approximately an equi-SHGC contour. While it is obvious that the east and west orientations are related by symmetry, and hence only one will need to be presented, it is also true that in these orientations the trajectories are nearly orthogonal to the contours, and thus show the most rapid variation. These variations could have a substantial effect on solar heat gain and on building loads.

Table 4 lists the resulting hourly SHGC values, as they might be presented in a handbook format.

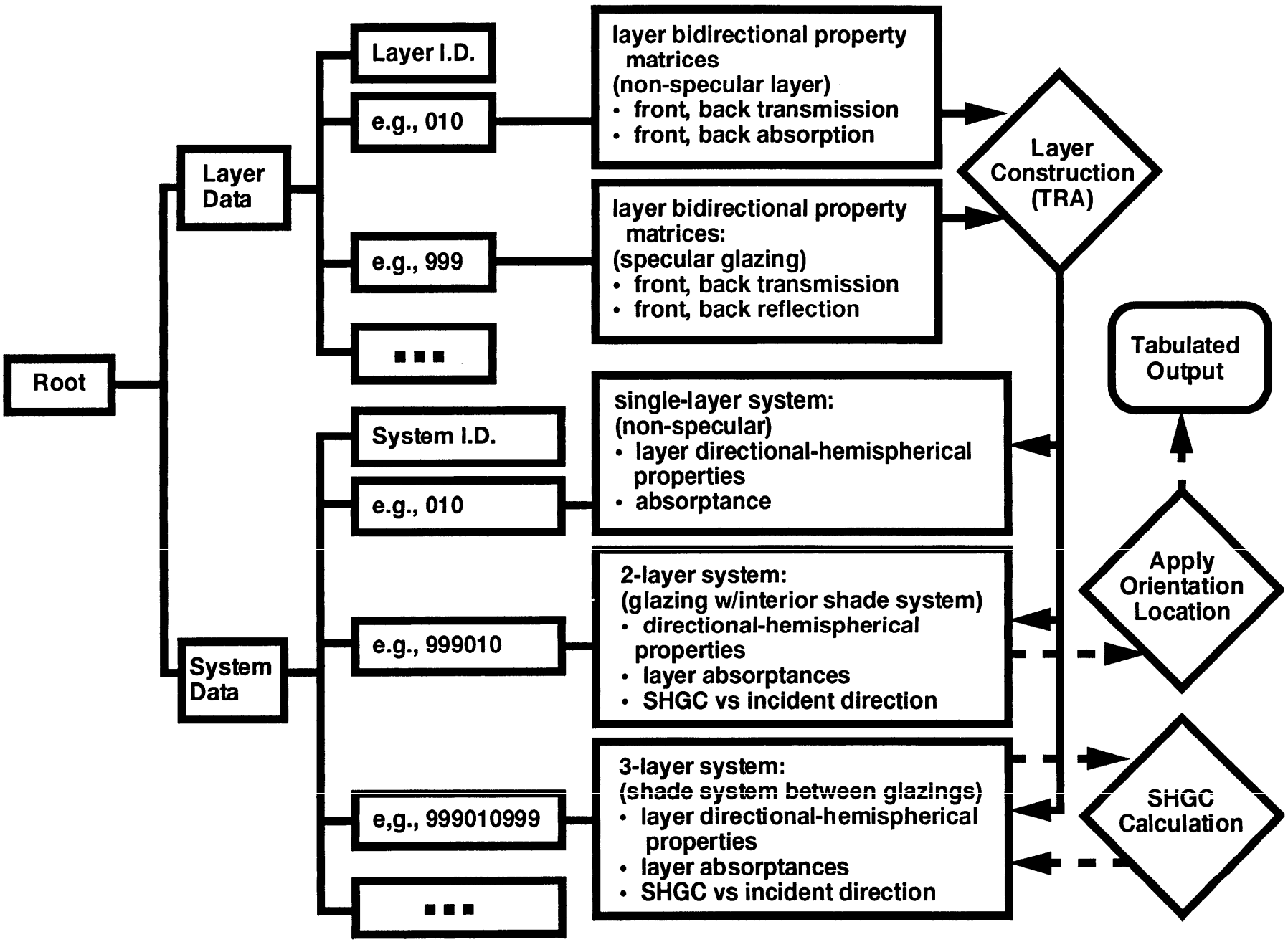

Figure 13. Data Base Directory Structure and its Interaction with Processing Calculations (Programs).

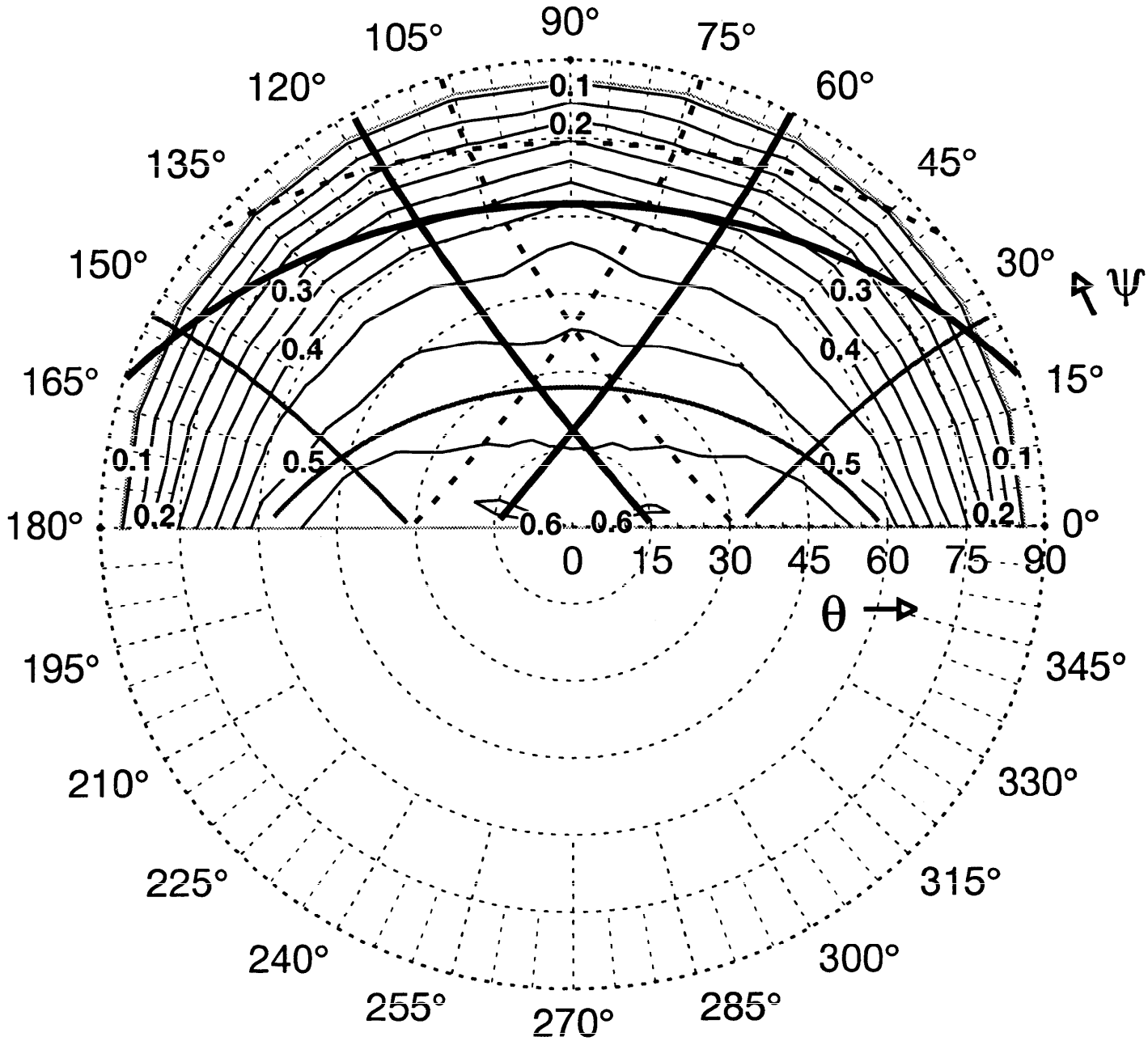

Figure 14. Sun Trajectories and Their Relation to SHGC Values. On the polar contour plot of Fig. 10 are plotted the sun trajectories at the equinox and the summer and winter solstices as seen in the east-, south- and west-facing orientations at 40 degrees north latitude. The curves for the south-facing orientation span both the first and second quadrants in ψ, while those for the east-facing quadrant rise to large values of θ in the second quadrant ($\psi > 90°$), while the mirror-image curves for west-facing rise to large θ in the first quadrant ($\psi < 90°$). The equinox is identified by heavy curves, the winter solstice by lighter solid curves (which are still heavier than the SHGC contours), and the summer solstice by dashed curves.

Table 4. Double Glazing with Interior Shade, 45° Slat Tilt. 40° N. Latitude

Summer Solstace

Hour	Solar Angle Azimuth	Solar Angle Altitude	SHGC East	SHGC South	SHGC West
5.5	-113	9	0.58		
6.5	-104	20	0.54		
7.5	-96	31	0.51		
8.5	-86	43	0.49	0.09	
9.5	-74	54	0.43	0.12	
10.5	-56	65	0.29	0.20	
11.5	-24	72	0.11	0.24	
12.5	22	72		0.24	0.11
13.5	56	65		0.20	0.28
14.5	74	55		0.12	0.42
15.5	86	43		0.09	0.49
16.5	96	32			0.51
17.5	104	20			0.54
18.5	113	9			0.57

Spring Equinox

Hour	Solar Angle Azimuth	Solar Angle Altitude	SHGC East	SHGC South	SHGC West
6.5	-94	14	0.56		
7.5	-85	25	0.53	0.09	
8.5	-74	36	0.50	0.21	
9.5	-60	47	0.44	0.31	
10.5	-41	56	0.31	0.35	
11.5	-15	61	0.12	0.38	
12.5	16	61		0.38	0.13
13.5	42	55		0.35	0.32
14.5	61	46		0.30	0.45
15.5	74	36		0.20	0.50
16.5	85	24		0.09	0.53
17.5	95	13			0.56

Winter Solstace

Hour	Solar Angle Azimuth	Solar Angle Altitude	SHGC East	SHGC South	SHGC West
8.5	-47	11	0.54	0.53	
9.5	-35	18	0.46	0.53	
10.5	-22	24	0.31	0.52	
11.5	-7	27	0.11	0.52	
12.5	8	26		0.52	0.13
13.5	23	23		0.52	0.33
14.5	36	18		0.52	0.47
15.5	48	10		0.53	0.55

Conclusions

We have demonstrated that the layer calculation method, utilizing scanning photometer measurements, is a viable way of determining the performance of complex fenestration systems, produces data that agrees with the most advanced outdoor calorimeter measurements that have yet been done, and allows the application of a data base incrementally to a wide variety of systems. Accumulating the data base is admittedly an arduous process, but we have now accumulated a set of the most time-consuming measurements--those of inward-flowing-fractions--that should allow the treatment of most of the common systems currently in use.

This points the way to a radically new way of approaching complex fenestrations, where the calorimetry is essentially done and the emphasis is on making the appropriate solar-optical measurements. A considerable variety of methods for making these methods exist or are conceivable, and vary in complexity with the type of system.

The large amount of detailed data produced by the scanner appears to be important for obtaining an accurate characterization of the most optically complex fenestration elements such as venetian blinds. In fact, it appears that a finer angular grid than the 15° one used here may be desirable. Further investigation is warranted to determine the relation between the achievable accuracy and the simplification of measurement.

Further instrumentation work will be necessary to develop a method for dealing with the optical properties of the most complex fenestration elements in a manner that is rapid, accurate and cheap.

This project has not dealt with the question of spectral properties and whether the intermingling of angular and spectral dependences can significantly affect performance. In principle, one would expect this. Research is recommended to explore the practical importance of this issue.

It is something of a mystery (at least to these authors) why the inward-flowing fractions appear to be so independent of temperatures and weather conditions. This project had too broad an agenda to treat this issue in sufficient detail, and additional research is recommended. We note that it is likely to prove a demanding research task.

Acknowledgments

The authors are grateful for the efforts of Mark Spitzglas, who participated in the early stages of scanning radiometer design and construction, of Konstantinos Papamichael, who made important contributions to the conceptual and early software development of the project, and of Ramalingam Muthukumar, who assisted in the later development of the analysis software. The efforts of Dennis DiBartolomeo, Mary Hinman, Jonathan Slack, and Mehrangiz Yazdanian were vital to the completion and automation of the scanning radiometer, and to support of the MoWiTT facility. Special thanks are due to the MoWiTT operational team, Steve Lambert and Michael Streczyn, whose patient and continuous efforts over several years resulted in the inward-flowing fraction measurements.

This research was jointly supported by ASHRAE, as Research Project 548-RP under Agreement No. BG 87-127 with the U.S. Department of Energy, and by the Assistant Secretary for Conservation and Renewable Energy, Office of Building Technologies, Building Systems and Materials Division of the U.S. Department of Energy under Contract No. DE-AC03-76SF00098.

References

Farber, E. A., W. A. Smith, et al. (1963). "Theoretical Analysis of Solar Heat Gain Through Insulating Glass with Inside Shading." ASHRAE Trans. **69**: 392.

Klems, J. H. (1994A). "A New Method for Predicting the Solar Heat Gain of Complex Fenestration Systems: I. Overview and Derivation of the Matrix Layer Calculation." ASHRAE Trans. **100**(pt. 1): pp. 1065-1072.

Klems, J. H. (1994B). "A New Method for Predicting the Solar Heat Gain of Complex Fenestration Systems: II. Detailed Description of the Matrix Layer Calculation." ASHRAE Trans. **100**(pt.1):

Klems, J. H. and G. O. Kelley (1995). "Calorimetric Measurements of Inward-Flowing Fraction for Complex Glazing and Shading Systems." ASHRAE Trans.: to be published.

Klems, J. H., S. Selkowitz, and S. Horowitz (1982). A Mobile Facility for Measuring Net Energy Performance of Windows and Skylights. Proceedings of the CIB W67 Third International Symposium on Energy Conservation in the Built Environment. Dublin, Ireland, An Foras Forbartha. 3.1.

Klems, J. H. and J. L. Warner (1992). A New Method for Predicting the Solar Heat Gain of Complex Fenestration Systems. Thermal Performance of the Exterior Envelopes of Buildings V, Clearwater Beach, FL, American Society of Heating, Refrigerating and Air-Conditioning Engineers, Inc.

Klems, J. H. and J. L. Warner (1995). "Measurement of Bidirectional Optical Properties of Complex Shading Devices." ASHRAE Trans. **101**(pt. 1); Symposium Paper CH-95-8-1); pp 791-801.

Klems, J. H., J. L. Warner, and G. O. Kelley (1995). "A Comparison between Calculated and Measured SHGC for Complex Glazing Systems." ASHRAE Trans.: to be published.

Rubin, M. (1985). "Optical Properties of Soda Lime Silica Glasses." Solar Energy Materials **12**: 275-288.

Yellott, J. I. (1966). "Shading Coefficients and Sun-Control Capability of Single Glazing." ASHRAE Trans. **72**: 72.